Strain Rate Effects of Nuclear Steels in Room and Higher Temperatures

Solomos G., Albertini C., Labibes K., Pizzinato V., Viaccoz B.

European Commission, Joint Research Centre, Institute for Systems, Informatics and Safety, I-21020 Ispra (VA), Italy

ABSTRACT

An investigation of strain rate, temperature and size effects of three nuclear steels has been undertaken. The materials are: ferritic steel 20MnMoNi55 (vessel head), austenitic steel X6CrNiNb1810 (Upper Internal Structure), and ferritic steel 26NiCr Mo146 (bolting). Smooth cylindrical tensile specimens of three sizes have been tested at strain rates from 0.001/s up to 300/s, at room and elevated temperatures (400^{o}C-600^{o}C). Full stress-strain diagrams have been obtained, and additional parameters have been calculated based on them. The results demonstrate a clear influence of temperature, which amounts into reducing substantially mechanical strengths with respect to R.T. conditions. The effect of strain rate is also shown. It is observed that at R.T. the strain rate effect causes up-shifting of the flow stress curves, whereas at the higher temperatures a mild down-shifting of the flow curves is manifested. Size effect tendencies have also been observed. Some implications when assessing the pressure vessel structural integrity under severe accident conditions are considered.

INTRODUCTION

Impact problems, like that of a slug of molten corium and debris on the upper head of the reactor vessel due to a hypothetical steam explosion, require a correct knowledge of the material deformation and failure processes. Investigations with small specimens should make sure that the results are transferable to the real problem and that the essential effects are adequately simulated. These effects include: size, strain rate, and temperature [1].

This research area has been given early attention and dealt with in the past [2-6]. Within the EU project REVISA some additional topics, primarily centered on the size effect issue, have been addressed. The Transient Dynamics sector of the Joint Research Centre has been assigned to carry out mainly the dynamic tests for material characterization, employing the Large Dynamic Test Facility (LDTF), which allows the testing of large specimens under well-defined strain rates. Several types of specimens have been foreseen of the materials used for the pressure vessel and its internal structures. These include: ferritic steel 20MnMoNi55 (vessel head), austenitic steel X6CrNiNb1810 (Upper Internal Structure), and ferritic steel 26NiCr Mo146 (bolting). Testing has been carried out at room and higher temperatures, and at strain rates ranging from quasi-static (10^{-3}/sec) to dynamic (300/sec) conditions. Uniaxial tensile cylindrical specimens of diameters ranging from 3mm to 30mm have been constructed. The size effect related activity has aimed principally at identifying real effects, and is only briefly reported herein [1] (see also Malmberg et al., paper 1224, division F of this conference).

EXPERIMENTAL TECHNIQUES AND SPECIMENS

Tensile tests at the several strain rates have been carried out by means of different machines: an old type Hounsfield screw tensometer, hydro-pneumatic apparatuses, small Hopkinson bars, servo-hydraulic machines, and the Large Dynamic Test Facility (LDTF). However, it is to be emphasized that identical data analysis procedures have been applied to all tests. Particular attention has been paid into producing comparable results in the dynamic regime for small and large specimens, and a range of split Hopkinson bar devices has been employed. Temperature tests have been conducted by using in-house made and commercial ovens with resistance heating. Special care has been taken of cooling down the Hopkinson bar ends in order to avoid alterations in the wave propagation parameters.

It is noted that the specimens used are not standard type tensile specimens; they are shorter and they are particularly adapted for dynamic testing at the Hopkinson bar. The ratio of uniform-section length to diameter is 1.67. They are geometrically similar, as illustrated in Figure 1, and of diameters ∅3, ∅9, ∅18 and ∅30mm. The target strain rates have been set at the following four levels: 10^{-3}/s, 10^{-1}/s, 10/s, and 200/s. A preliminary analysis of the slug impact has indicated that no higher strain rates should be expected in such an event.

As mentioned above, uniaxial tests at high strain rate were performed on a modified Hopkinson bar device [7], shown schematically in Figure 2. It consists of two half-bars, the incident and transmitter bar respectively, with the specimen introduced in between. Elastic energy is stored in a pre-stressed bar, which is the solid continuation of the incident bar of the machine. By releasing this energy (rupturing the blocking brittle intermediate piece), a tension wave with small rise-time is generated and transmitted along the incident bar loading the specimen to fracture. This tension wave fulfils the requirements for being a uniaxial elastic plane stress wave because (i)the pulse wave length is long compared to the bar diameter, and (ii)the pulse amplitude does not exceed the yield strength of the bar.

The pulse propagates along the incident bar with the velocity C_o of the elastic wave with its shape remaining constant [8]. When the incident pulse (ε_I) reaches the specimen, part of it (ε_R) is reflected by the specimen whereas another part (ε_T) passes through the specimen propagating into the transmitter bar. The relative amplitudes of the incident, reflected and transmitted pulses, depend on the mechanical properties of the specimen.

Fig.1 The ∅3, ∅9 and ∅30mm specimens used in this study.

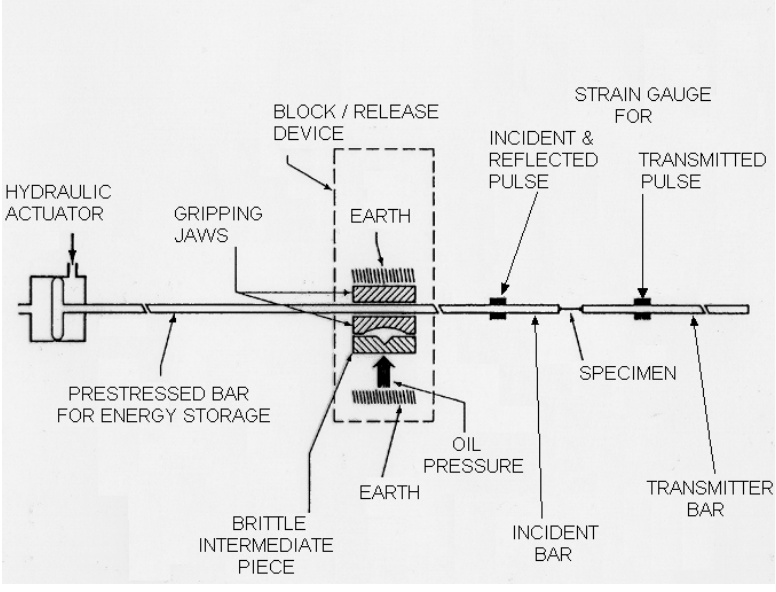

Fig.2 The JRC modified tension Hopkinson bar.

Strain gauges mounted on the incident and transmitter bars of the device, at equal distances from the specimen, are used for the measurement of the elastic deformation (as a function of time) created on both half-bars by the incident/reflected and transmitted pulses, respectively. Using the theory of elastic wave propagation in bars [8], and the well substantiated assumption of specimen equilibrium attainment, the engineering stress σ_E, strain rate $\dot{\varepsilon}_E$, and strain ε_E of the specimen can be calculated:

$$\sigma_E(t) = E_b\, \varepsilon_T(t)\, \frac{A_b}{A_o} \tag{1}$$

$$\dot{\varepsilon}_E(t) = \frac{2C_o}{L_c}\varepsilon_R(t) \quad , \qquad \varepsilon_E(t) = \frac{2C_o}{L_c}\int_0^t \varepsilon_R(z)dz \tag{2}$$

where, L_c= corrected gauge length of the specimen (see below), A_b= cross-sectional area of output and input bars, A_o= initial cross-sectional area of the specimen gauge length portion, E_b=elastic modulus of the bars, C_o= $(E_b/\rho)^{1/2}$ the elastic bar wave speed, ρ = bar density.

Since dynamic testing of big specimens is central to this activity, it is also worth providing some further information about the LDTF. Its principle is based on that shown in Fig.2, where, however, the prestressed energy storage bar consists of 32 steel cables of 100m length and ~3200mm^2 total cross-sectional area. In its basic configuration, the incident and transmitter bars are solid bars of 72mm diameter, with the length of the transmitter bar being 100m. A rectangular stress pulse of maximum amplitude ~2.5MN and of duration 40ms can be potentially generated. Thus, with a maximum stroke of ~750mm this machine can bring to fracture very big specimens and components of ductile materials.

For all tests a few elongation measurements have been made directly on the initial gage length L_o, which is usually made to coincide with the length of the uniform section. What is always measured and recorded is the relative displacement ($\Delta\ell$) of the specimen two extremes (gripping bar ends, or machine cross-head displacement). Consequently, the gauge length L_o is corrected to take into account the contribution to the measured elongation of the two deformable fillets of the tensile specimen [9]. This correction is carried out by measuring the deformation of the length between two inner marks (L_o) and between two outer marks (L), with the use of a microscope. Considering that the volume of the gauge part of the specimen remains constant during the experiment, the corrected gauge length L_c is calculated through the following formula [1,7]:

$$L_c = L_o \frac{\Delta L_f}{\Delta L_{of}} \tag{3}$$

where, L_c = corrected specimen gauge length, ΔL_{of} = elongation at fracture over the central gauge length L_o, and ΔL_f = elongation at fracture over the length L.

Stress-strain diagrams obtained with the different experimental set-ups have been re-adjusted by imposing a correct Young modulus [7]. This correction is necessary because the experimental elastic modulus determined from these tests is not accurate. At high strain rates the specimen takes a certain finite time to achieve equilibrium along its gauge length [8], and in the case of the tests at low and medium strain rates the experimental elastic modulus may be affected by the deformation of the dynamometric elastic bars. This final procedure yields the engineering strain values ε_E to be used in the diagrams.

Examination of the specimens has also been made after fracture. The specimens are at best reconstructed by bringing together the two broken parts, and for the majority of the tests the diameter and the meridional radius of curvature at the reduced section have been measured. Subsequently the last point of the true stress-strain diagram has been determined by using the Bridgman correction formula [1] for the stress.

EXPERIMENTAL RESULTS

Austenitic Steel X6CrNiNb1810 (1.4550)

This is the material of the Upper Internal Structure (UIS). The specimens have been constructed at the Paul Scherrer Institut (CH) from material delivered in four plates of dimensions 1000x300x70(mm) coming from the same heat. A limited scope quality control has been conducted and completed, mainly concentrating on chemical composition, grain size determination and hardness tests. Inhomogeneities, which are typical to austenitic steels, have been encountered [10]. Brinnel-hardness values across the thickness of the plates have also been found lower than those on the surface along the longitudinal direction. Thus some positional influences are likely to be encountered.

Experiments have been performed with ∅3, ∅9 and ∅30mm cylindrical specimens, according to the pre-established test matrix, at room temperature and at 600^{o}C, at the predefined target strain rates. Approximately 65 specimens have been used. Produced strain rates have been slightly different. All corresponding stress-strain curves (both engineering and true) have been obtained [1]. For the reasons explained before, the Young modulus of these curves has been adjusted to 200GPa for R.T. and to 165GPa for 600^{o}C, respectively [11].

Figure 3 shows typical complete σ–ε curves of the ∅3mm specimens. It can be seen that the material has an overall strain hardening behaviour. Figure 4 shows the ultimate strength values for all three specimen sizes over the strain rate domain for the two test temperatures.

At room temperature and with increasing strain rate the flow stresses tend in general to increase. Both the ultimate tensile strength and the yield stress present a small but constant increasing trend with strain rate. It is also noticed that for all three specimen sizes at the 200/s strain rate an instability (upper and lower yield points) appears, which does not exist at the static straining. Both the uniform and the fracture strains decrease with increasing strain rates (especially for the ∅3mm specimens), and the material seems to lose ductility.

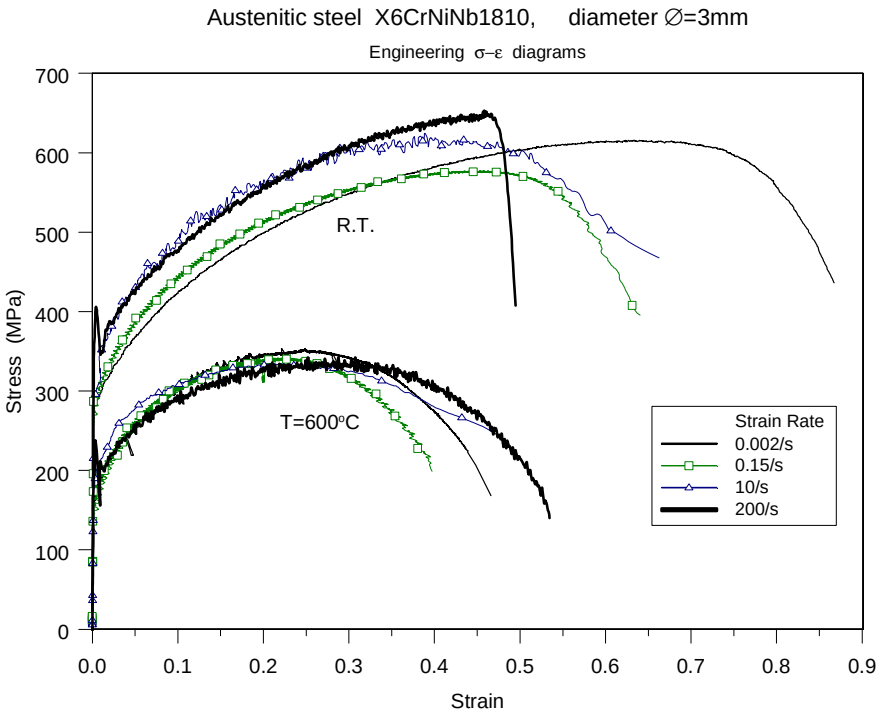

Fig.3 Typical stress-strain curves for several strain rates and two temperatures.

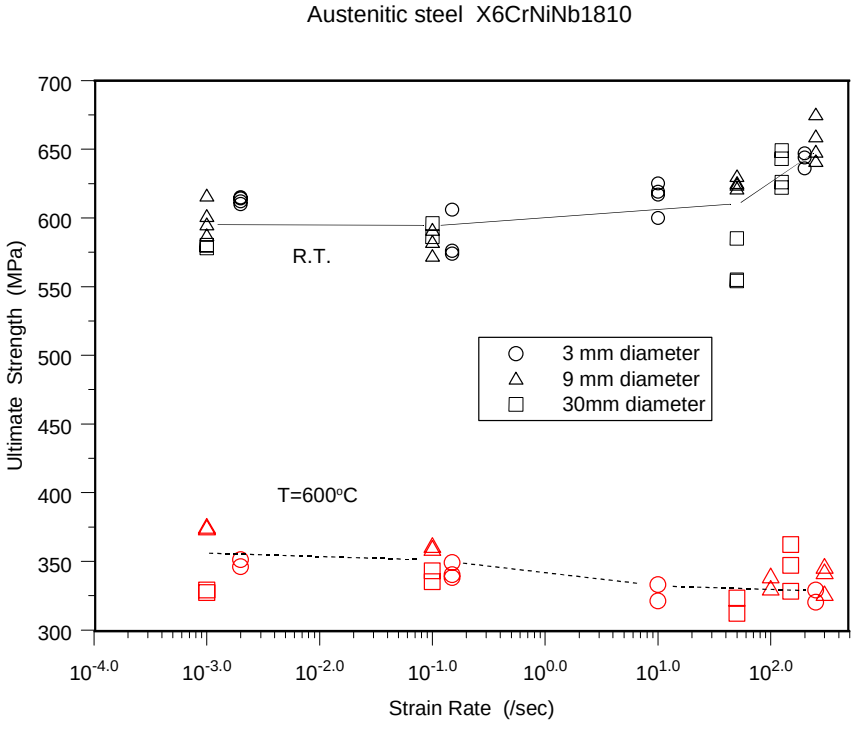

Fig.4 Behaviour of the tensile strength against strain rate for three specimen sizes and two temperatures.

At temperature T=600°C and with increasing strain rate no strong strain rate effects appear. The flow stresses in general remain invariant with a small tendency towards decreasing. As shown also in Fig.4, the tensile strength undergoes a small

decrease. As at room temperature, for the 200/s strain rate the yield point instability appears again for all three specimen sizes. Apart from this, the yield stress remains almost invariant with strain rate. The uniform and fracture strains show a small increase with strain rate, as if the material at this temperature becomes more ductile under dynamic straining.

As clearly shown through these figures, at 600°C a substantial reduction of the mechanical resistance and ductility is observed with respect to R.T. conditions for all strain rate regimes and all specimen sizes. Some average values illustrate the situation at this temperature: tensile strength 300MPa (down from 600MPa at R.T.), uniform strain 0.25 (down from 0.50), fracture strain 0.45 (down from 0.80), yield stress 160MPa (down from 350MPa).

Ferritic Steel 20MnMoNi55 (1.6310)

This is the vessel head material. The relevant specimens have been constructed at PSI from material delivered in plates of dimensions 1000x500x70(mm). Six of them were used for an extensive material quality assurance verification [12]. This comprised chemical analysis, metallographic investigations, hardness tests, tensile tests and Charpy impact tests. The results indicated an overall good material state with moderate variations over the plates. They also revealed the existence of a noticeable positional influence with regards to the mechanical properties, mainly concentrated along the plates' length, but also across their thickness [1,12].

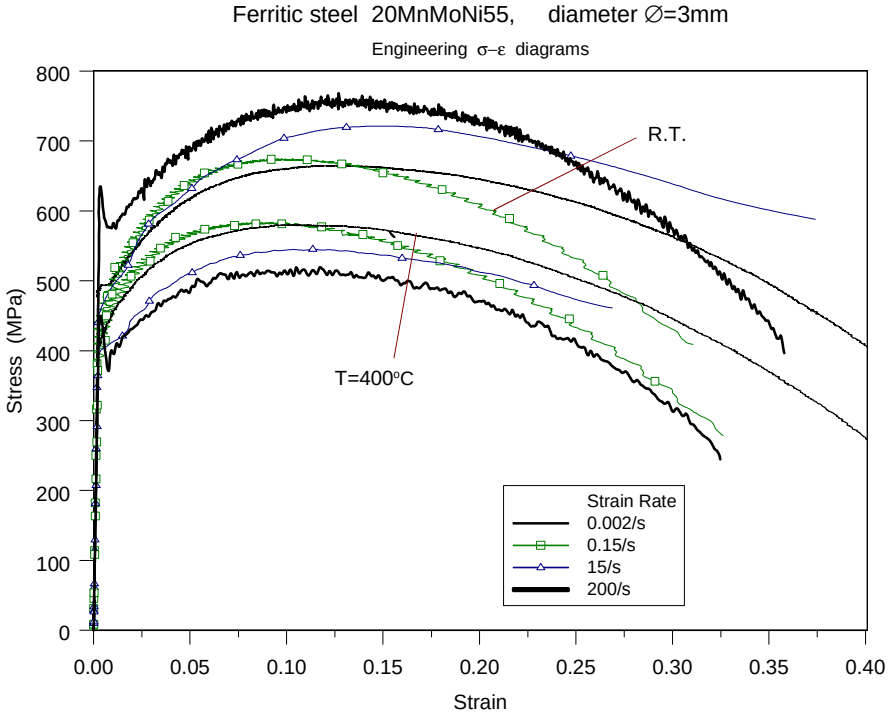

Fig.5 Typical stress-strain curves for several strain rates and two temperatures.

Experiments have been performed with ∅3, ∅9 and ∅30mm cylindrical specimens, according to the pre-established test matrix, at room temperature and at 400°C, at the predefined target strain rates. A total of 70 specimens were used. As previously, produced strain rates have been slightly different. All corresponding stress-strain curves (both engineering and true) have been obtained. The small sub-set of the engineering curves is used in Figure 5 for comparison purposes. The Young modulus of these curves has been adjusted to 200GPa for R.T. and to 165GPa for 400°C, respectively. Figure 5 shows typical σ–ε curves of the ∅3mm specimens. It can be seen that strain hardening behaviour is overall prevalent.

At room temperature and with increasing strain rate the flow stresses tend always to increase. Both the ultimate tensile strength and the yield stress present a significant increase with strain rate. This material exhibits a yield instability (upper and lower yield points) even at static straining. However, it is observed that for all three specimen sizes at the higher strain rates this phenomenon is further accentuated with a distinct upper and lower yield point. The ductility of the material does not seem to be sensitive to strain rate.

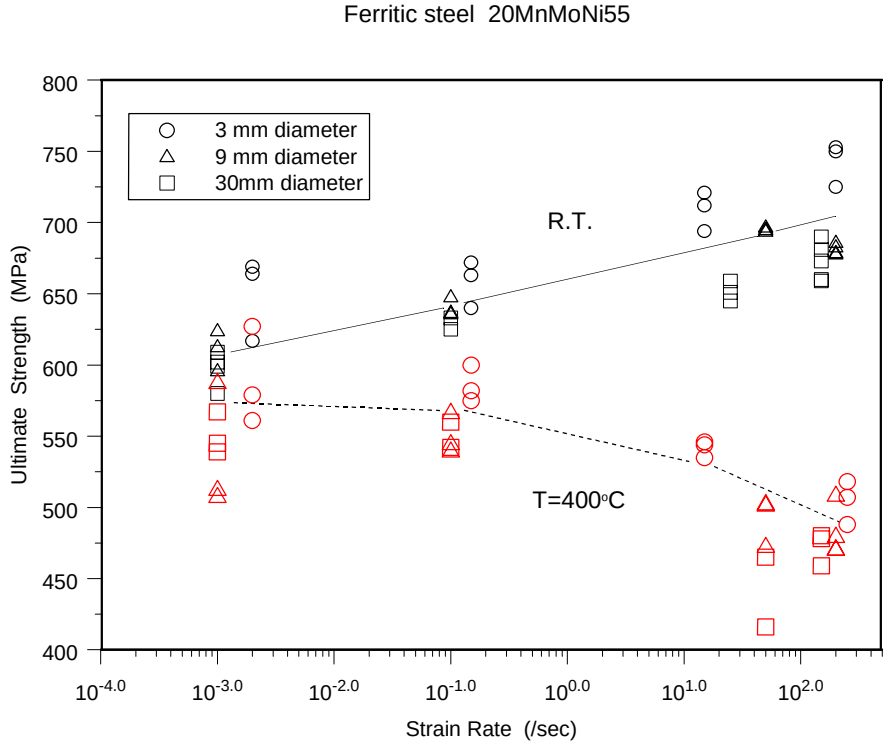

Fig.6 Behaviour of the tensile strength against strain rate for three specimen sizes and two temperatures.

At temperature T=400°C and with increasing strain rate noticeable strain rate effects appear. The flow stresses in general remain invariant with a tendency towards decreasing. As shown also in Fig.6, the tensile strength undergoes a small decrease, whereas the yield stress remains almost invariant. It is worth noting that at this temperature no yielding instability is present for static straining. However, for the 200/s strain rate the yield point instability appears again for all three specimen sizes. As for the room temperature, the ductility of the material does not seem to be sensitive to strain rate.

As clearly shown through Figs.5-6, at 400°C a reduction of the mechanical resistance is observed with respect to R.T. conditions for all strain rate regimes and all specimen sizes. The ductility does not appear to be affected. Due to the differing strain hardening effects at R.T. and at T=400°C, it is evident that the big differences are manifested at the higher strain rates. To illustrate this situation some average values are quoted: tensile strength at 0.001/s is 590MPa (down by ~10% from 650MPa at R.T.); tensile strength at 200/s is 505MPa (down by ~30% from 743MPa at R.T.).

Ferritic Steel 26NiCrMo146 (1.6958)

This is the material of the bolts used for fixing the vessel head onto the top of the cylindrical reactor vessel. Specimens have been constructed by the JRC from two different heats of material furnished by FZKarlsruhe. Heat 1 includes 15 unused bolts (of the BERDA experiment), and heat 2 a half-cylinder of 340mm diameter and 180mm height. The dimensions of these sources have dictated the choice of the maximum specimen size of ∅18mm. Some specimens of ∅3, ∅9mm have been constructed from both heats, so as to investigate any material production variation effects. No quality assurance tests have been carried out.

Experiments have been conducted, according to a pre-established test matrix, only at room temperature with the above size specimens at the predefined target strain rates. All corresponding stress-strain curves (both engineering and true) have been obtained, and the Young modulus of these curves has been adjusted to 200GPa.

It is to be noted that for all strain rate regimes the material has a high elastic limit and yield point (over 1000MPa), which lie close to the tensile strength (average 1200MPa). Further, it exhibits a quite short plastic deformation (fracture strain not exceeding 0.25). As the relevant σ–ε curves show, the material exhibits a strain hardening behaviour. At room temperature and with increasing strain rate the flow stresses have a weak tendency to increase. Specifically, the ultimate tensile strength exhibits a net increase with strain rate, Figure 7, whereas the yield stress presents no significant change. No yield instability is observed, and the ductility does not seem to be sensitive to strain rate.

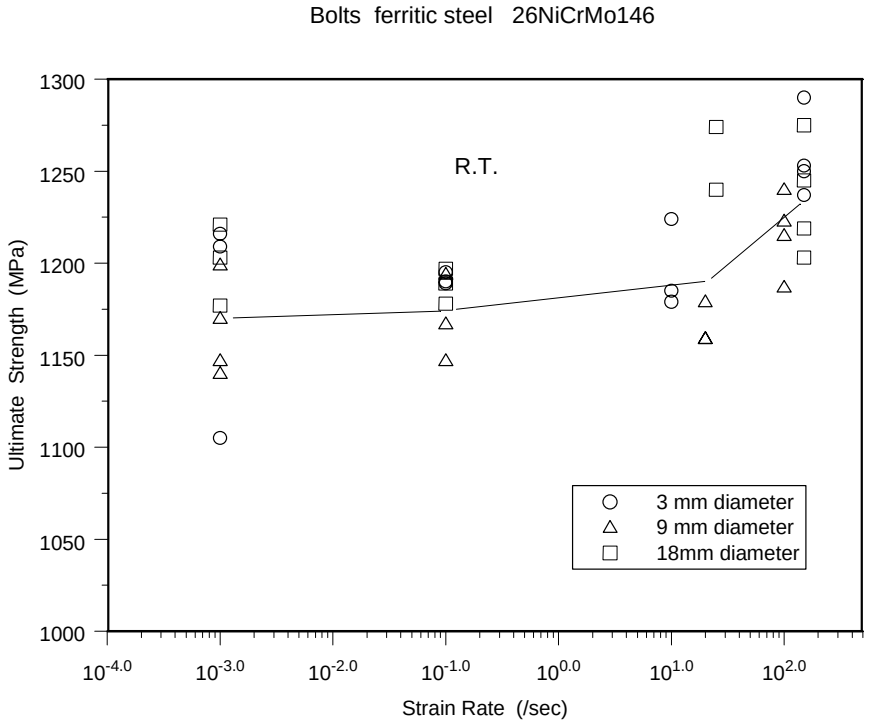

Fig.7 Behaviour of the tensile strength against strain rate for three specimen sizes at R.T.

DISCUSSION-CONCLUSIONS

A large experimental campaign consisting of tensile tests of three nuclear steels has been carried out. These are the ferritic steel 20MnMoNi55 of the vessel head, the austenitic steel X6CrNiNb1810 of the Upper Internal Structure, and the ferritic steel 26NiCr Mo146 of the bolts. Smooth cylindrical specimens of diameters ranging from 3mm to 30mm have been tested at strain rates from 0.001/s up to 300/s. Room and higher temperatures up to 600^{o}C have been applied. Basic objective has been the investigation of strain rate, temperature and size effects of these materials.

Stress-strain diagrams, both engineering and true, have been obtained for each test. Measurements of specimen geometrical parameters have been made before and after the test, and additional parameters have been calculated based on the σ–ε curves. By combining and properly plotting this data it has been attempted to examine the existence and to assess the order of magnitude of each of the above effects, where possible.

The results amply demonstrate the degrading influence of temperature; mechanical strengths at 400^{o}C-600^{o}C are reduced by as much as 30% with respect to R.T. conditions. Also shown characteristically is the effect of strain rate, of varying degree for each material. It has been observed that at R.T. the strain rate effect causes an upwards shift of the flow stress curve (strength increase with strain rate by as much as 20%). However, at T=600^{o}C for the X6CrNiNb1810 steel and at T=400^{o}C and for the 20MnMoNi55 steel, respectively, it results in smaller flow stresses and is accompanied by ductility reduction. This behaviour at higher temperatures should probably be attributed to the adiabatic conditions of loading, which become even more accentuated at elevated temperatures, thus rendering the thermal softening dominant [13,14].

Size effect tendencies have also been noticed. The relevant graphs have not been presented due to paper space limitations. Seemingly, strength resistance of small specimens tends to be greater than that of the big specimens. However, the situation is particularly sensitive when dealing with the size effect issue. Before any trends can be declared as true size effect, all possible error sources must have been eliminated. In the specific case, from the quality assurance of the original steel plates it is already known that there exist positional influences, which could potentially be masked as size effects. They could also alter the quantification of the temperature and strain rate effects. This important issue has not been explicitly raised in the preceding discussion. For example, a preliminary analysis in associating mechanical specimen properties and specimen position in the original plate has been undertaken in [15], where it has been demonstrated that size effects in strength parameters can practically be discarded. More consistent size effect evidence constitutes the behaviour of the area reduction

parameter and of the normalized meridional radius of curvature at fracture, both of which are local quantities. As repeatedly verified by the tests, the normalised radius of curvature parameter is monotonically increasing, and the area reduction parameter monotonically decreasing with increasing specimen size. In both cases this means that the smaller the specimen, the bigger the deformation concentration is at fracture.

As regards the more concrete results of this study on strain rate and temperature effects, it is considered that they can have important implications when assessing the pressure vessel structural integrity under impact accident conditions. It has been found that the ferritic steel 20MnMoNi55 and the austenitic steel X6CrNiNb1810 have a peculiar dynamic behaviour at temperatures from 400^{o}C to 600^{o}C, which overall amounts to a reduction of strength for higher strain rates. Clearly, this behaviour must be properly reflected and introduced in the constitutive relations of the material if the relevant structural analysis codes are to produce reliable simulations. However, attention is drawn to the fact that these findings are limited to the 200/s strain rate, and refer to the specific temperatures cited above, which are below the respective recrystallization points. Beyond the recrystallization temperature, the ratio of the dynamic to quasi-static flow stresses usually becomes more sensitive to temperature and may show a rapid increase [16]. For this reason it is essential to establish reliable accident scenarios with the associated temperatures and impact induced strain rates, and carry out the dynamic characterisation of the material under these conditions.

REFERENCES

1. Solomos, G., Albertini, C., Labibes, K., Pizzinato, V., Viaccoz, B., Delzano, C., Schnabel, W., "Experimental investigation of Strain Rate, Temperature and Size Effects in Nuclear Steels", Work performed within EU Project REVISA (FI4S-CT96-0024), Technical Note No.I.00.76, JRC Ispra, June 2000.
2. Wood, D.S., Duwez, P.E. and Clark, D.S., "The influence of specimen dimensions and shape on the results of tensile impact tests", Armor and Ordnance report No. A-237 (OSRD No. 3028), 1943.
3. Miklowitz, J., "The influence of the Dimensional Factors on the Mode of Yielding and Fracture in Medium-Carbon Steel –I, The Geometry and Size of the Flat Tensile Bar", *J. Applied Mechanics*, Trans. ASME, vol.70, pp.274-287, Sept.1948.
4. Miklowitz, J., "Influence of the Dimensional Factors on Mode of Yielding and Fracture in Medium-Carbon Steel –II, The Size of the Round Tensile Bar", *J. Applied Mechanics*, pp.159-168, June 1950.
5. Richards, C.W., "Effect of size on the yielding of mild steel beams", *Proc. Am. Soc. Testing Mater.*, Vol.58, pp.955-970, 1958.
6. Malmberg, T., "Aspects of similitude theory in Solid Mechanics, Part I: Deformation Behavior", Forschungszentrum Karlsruhe, Scientific Report FZK 5657, Dec.1995.
7. Albertini, C. and Montagnani, M., "Dynamic material properties of several steels for fast breeder reactor safety analysis", EUR 5787 EN, Ispra,1977.
8. Lindholm, U.S., "High strain rate tests", in *Techniques of Metals Research*, Vol. V, Part l, R.F. Bunsmah editor, J. Wiley & Sons, 1971.
9. Nicholas, T., "Tensile Testing of Materials at High Rates of Strain", *Experimental Mechanics*, pp.177-185, 1981.
10. Krompholz, K., "Quality assurance of the Austenitic steel X6CrNiNb1810", PSI report TM-49-98-07.
11. Stainless steels; quality specifications, DIN 17 440, Dec.1972.
12. Krompholz, K., Kamber, J., Kalkhof, D., "A preliminary study of material homogeneity for size effect investigations", PSI report Nr.99-03, June 1999.
13. Zener, C., Hollomon, J.H., "Effect of strain rate upon the plastic flow of steel", *J. Appl. Phys.*, 15, pp.22-32, 1944.
14. Dodd, B., Bai, Y., *Ductile fracture and ductility*, Academic Press, 1987.
15. Malmberg, T., Krompholz, K., Solomos, G., Aifantis, E.C., "Investigation on size effects in ferritic and austenitic materials", *Proc. SMiRT-15*, Seoul Korea, August 15-20, 1999.
16. Johnson, W., *Impact Strength of Materials*, Arnold, London, 1972.

AKNOWLEDGEMENTS

This study has been performed within the project REVISA "Reactor Vessel Integrity in Severe Accidents" of the EU Nuclear Fission Safety / Reactor Safety Programme. The EU financial support is gratefully acknowledged. Special thanks are also due to Dr. K.Krompholz, of PSI, for kindly helping out with some quasi-static tests of the big specimens, and to Dr. T.Malmberg, of FZK, for his continuous interest and fruitful interaction in the course of the work.